AIMS Mathematics, 11(4): 9989–10003.
DOI: 10.3934/math.2026412
Received: 05 February 2026
Revised: 20 March 2026
Accepted: 27 March 2026
Published: 14 April 2026

https://www.aimspress.com/journal/Math

Research article

A second-order linear energy-stable scheme for slope-selection epitaxial thin-film growth

Hyun Geun Lee*

Department of Mathematics, Dongguk University, Seoul 04620, Republic of Korea

* **Correspondence:** Email: leeh1@dongguk.edu.

Abstract: The slope-selection epitaxial thin-film growth model was formulated as the L^2-gradient flow of an energy functional with a nonlinear potential of the surface slope. We developed a second-order, linear, and energy-stable scheme for this model based on a linear convex splitting in which the nonlinear potential term was treated explicitly together with an auxiliary term that ensured the convexity of the explicit part. The scheme was constructed using a second-order strong-stability-preserving implicit–explicit Runge–Kutta method. We explicitly identified the range of Runge–Kutta coefficients for which the original discrete energy decay property held, and proved that the scheme was unconditionally energy-stable with respect to the original discrete energy functional. Numerical results were presented to verify the accuracy, computational efficiency, and long-time energy stability of the scheme.

Keywords: epitaxial thin-film growth; slope selection; linear convex splitting; second-order strong-stability-preserving implicit–explicit Runge–Kutta; energy stability
Mathematics Subject Classification: 65M06, 65N06

1. Introduction

The slope-selection epitaxial thin-film growth model describes the morphological evolution of thin-film surfaces during epitaxial deposition by favoring a specific slope. It is formulated as the L^2-gradient flow of the energy functional [1]

$$\frac{\partial \phi}{\partial t} = -\frac{\delta \mathcal{E}}{\delta \phi}, \quad \frac{\delta \mathcal{E}}{\delta \phi} = -\nabla \cdot (|\nabla \phi|^2 \nabla \phi) + \Delta \phi + \delta \Delta^2 \phi \tag{1.1}$$

with

$$\mathcal{E}(\phi) = \int_\Omega \left(\frac{1}{4}(|\nabla \phi|^2 - 1)^2 + \frac{\delta}{2}|\Delta \phi|^2 \right) d\mathbf{x}. \tag{1.2}$$

Here ϕ is the scaled height function of the thin film in a co-moving frame, $\delta > 0$ is a constant, $\frac{\delta}{\delta\phi}$ denotes the variational derivative, and periodic boundary conditions are imposed in all spatial directions. The first term in (1.2) selects the slope of the film surface. For this reason, Eq. (1.1) is referred to as the growth equation with slope selection (SS equation), which satisfies the energy decay property.

The physically interesting coarsening dynamics occur over very long time scales. The SS equation predicts $\mathcal{E}(t) \sim O(t^{-\frac{1}{3}})$ and $w(t) \sim O(t^{\frac{1}{3}})$ as $t \to \infty$ [1–3], where $w(t)$ is the roughness defined by

$$w(t) = \sqrt{\frac{1}{|\Omega|}\int_\Omega \left(\phi(\mathbf{x},t) - \frac{1}{|\Omega|}\int_\Omega \phi(\mathbf{x},t)\,d\mathbf{x}\right)^2 d\mathbf{x}}\,.$$

Therefore, numerical simulations of the coarsening dynamics require long-time accuracy and energy stability. Various second-order and energy-stable schemes have been proposed to solve the SS equation. In [4], Shen et al. constructed the second-order convex splitting scheme by combining the convex splitting idea [5] and the secant method [6], where the energy stability was established with respect to the following modified discrete energy functional:

$$\tilde{\mathcal{E}}(\phi^{n+1},\phi^n) = \mathcal{E}(\phi^{n+1}) + \int_\Omega \frac{1}{4}|\nabla(\phi^{n+1}-\phi^n)|^2\,d\mathbf{x}.$$

In [7], Yang et al. developed the second-order backward differentiation formula based on the invariant energy quadratization method [8], where the energy stability was proved with respect to the following modified discrete energy functional:

$$\tilde{\mathcal{E}}(\phi^{n+1},\phi^n) = \int_\Omega \left(\frac{1}{4}\frac{(U(\phi^{n+1}))^2 + (2U(\phi^{n+1}) - U(\phi^n))^2}{2} + \frac{\delta}{2}\frac{(\Delta\phi^{n+1})^2 + (2\Delta\phi^{n+1} - \Delta\phi^n)^2}{2}\right)d\mathbf{x},$$

where $U(\phi) = |\nabla\phi|^2 - 1$. In [9], Feng et al. presented the second-order backward differentiation formula with a second-order Douglas–Dupont regularization, where the energy stability was established with respect to the following modified discrete energy functional:

$$\tilde{\mathcal{E}}(\phi^{n+1},\phi^n) = \mathcal{E}(\phi^{n+1}) + \int_\Omega \left(\frac{1}{4\Delta t}(\phi^{n+1}-\phi^n)^2 + \frac{1}{2}|\nabla(\phi^{n+1}-\phi^n)|^2\right)d\mathbf{x}.$$

In [10], Cheng et al. developed the second-order backward differentiation formula based on the scalar auxiliary variable approach [11], where the energy stability was proved with respect to the following modified discrete energy functional:

$$\tilde{\mathcal{E}}(\phi^{n+1},\phi^n) = \frac{(V(\phi^{n+1}))^2 + (2V(\phi^{n+1}) - V(\phi^n))^2}{2} + \int_\Omega \frac{\delta}{2}\frac{(\Delta\phi^{n+1})^2 + (2\Delta\phi^{n+1} - \Delta\phi^n)^2}{2}\,d\mathbf{x},$$

where $V(\phi) = \sqrt{\int_\Omega \frac{1}{4}(|\nabla\phi|^2 - 1)^2\,d\mathbf{x} + C}$ and $C > 0$ is a constant such that $\int_\Omega \frac{1}{4}(|\nabla\phi|^2 - 1)^2\,d\mathbf{x} + C > 0$.

In this paper, we develop a second-order, linear, and energy-stable scheme for the SS equation that preserves the decay of the original discrete energy functional, rather than a modified one, without sacrificing accuracy or computational efficiency. The proposed approach is based on a linear convex splitting of the original energy functional, in which the nonlinear potential term is treated explicitly together with an auxiliary term that ensures the convexity of the explicit part. The convex splitting

idea has been widely applied to various gradient flow equations. However, the standard convex splitting scheme leads to formally first-order accuracy. To improve its temporal accuracy, a variety of higher-order schemes have been developed, including those based on backward differentiation formulas [12] and implicit–explicit methods [13]. Here, we combine the proposed linear convex splitting with a second-order strong-stability-preserving implicit–explicit Runge–Kutta (SSP-IMEX-RK) method [14, 15] to achieve second-order temporal accuracy. Although all RK coefficients yield second-order temporal accuracy, they do not necessarily guarantee the decay of the original discrete energy functional. We explicitly identify the range of RK coefficients for which the original discrete energy decay property holds, and prove that the scheme is unconditionally energy-stable with respect to the original discrete energy functional.

This paper is organized as follows. In Section 2, we construct a second-order, linear scheme and establish the decay of the original discrete energy functional. In Section 3, numerical results are presented to verify the accuracy, computational efficiency, and long-time energy stability of the scheme. Section 4 concludes the paper. Appendix includes the MATLAB code for the scheme and additional spatial refinement tests.

2. Numerical scheme

To preserve energy stability without sacrificing computational efficiency, we consider the following splitting:

$$\begin{aligned}\mathcal{E}(\phi) &= \mathcal{E}_c(\phi) - \mathcal{E}_e(\phi)\\ &= \int_\Omega \left(\frac{\delta}{2}|\Delta\phi|^2 + \frac{A}{2}|\nabla\phi|^2\right)d\mathbf{x} - \int_\Omega \left(-\frac{1}{4}(|\nabla\phi|^2-1)^2 + \frac{A}{2}|\nabla\phi|^2\right)d\mathbf{x}. \end{aligned} \tag{2.1}$$

The convexity of $\mathcal{E}_c(\phi)$ is obvious for $A \geq 0$.

Lemma 1. *$\mathcal{E}_e(\phi)$ is convex if $A \geq 3\max_{\mathbf{x}\in\Omega}|\nabla\phi|^2 - 1$.*

Proof. The convexity of $\mathcal{E}_e(\phi)$ follows from the convexity of the function

$$F(\mathbf{u}) = -\frac{1}{4}(|\mathbf{u}|^2-1)^2 + \frac{A}{2}|\mathbf{u}|^2$$

with $\mathbf{u} = \nabla\phi$. A direct calculation gives

$$\nabla_{\mathbf{u}}F(\mathbf{u}) = (A+1-|\mathbf{u}|^2)\mathbf{u}, \quad \nabla^2_{\mathbf{u}}F(\mathbf{u}) = (A+1-|\mathbf{u}|^2)I - 2\mathbf{u}\mathbf{u}^T.$$

For any $\mathbf{v} \in \mathbb{R}^d$, we have

$$\mathbf{v}^T\nabla^2_{\mathbf{u}}F(\mathbf{u})\mathbf{v} \geq (A+1-3|\mathbf{u}|^2)|\mathbf{v}|^2.$$

Therefore, if $A+1 \geq 3\max_{\mathbf{x}\in\Omega}|\mathbf{u}|^2$, the Hessian is positive semi-definite, and, hence, $F(\mathbf{u})$ is convex. □

To achieve second-order temporal accuracy, we combine the linear convex splitting (2.1) with the second-order SSP-IMEX-RK method:

$$\begin{aligned}
\phi^{(1)} &= \phi^n - \Delta t\left(\frac{\delta \mathcal{E}_c(\phi^{(1)})}{\delta \phi} - \frac{\delta \mathcal{E}_e(\phi^n)}{\delta \phi}\right),\\
\phi^{(2)} &= a_{10}\phi^n + a_{11}\phi^{(1)} - b_1\Delta t\left(\frac{\delta \mathcal{E}_c(\phi^{(2)})}{\delta \phi} - \frac{\delta \mathcal{E}_e(\phi^{(1)})}{\delta \phi}\right),\\
\phi^{n+1} &= a_{20}\phi^n + a_{21}\phi^{(1)} + a_{22}\phi^{(2)} - b_2\Delta t\left(\frac{\delta \mathcal{E}_c(\phi^{n+1})}{\delta \phi} - \frac{\delta \mathcal{E}_e(\phi^{(2)})}{\delta \phi}\right),
\end{aligned}$$

where $\frac{\delta \mathcal{E}_c(\phi)}{\delta \phi} = \delta\Delta^2\phi - A\Delta\phi$ and $\frac{\delta \mathcal{E}_e(\phi)}{\delta \phi} = \nabla\cdot(|\nabla\phi|^2\nabla\phi) - (A+1)\Delta\phi$. We note that the convexity of $\mathcal{E}_c(\phi)$ is ensured for $A \geq 0$, while that of $\mathcal{E}_e(\phi)$ is ensured for $A \geq 3\max\limits_{\mathbf{x}\in\Omega}|\nabla\phi|^2 - 1$. Accordingly, for the first stage we take

$$A^n = 3\max_{\mathbf{x}\in\Omega}|\nabla\phi^n|^2,$$

which is computed from the known solution ϕ^n and satisfies the required convexity conditions at the first stage. Similarly, for the second and third stages we take

$$A^{(1)} = 3\max_{\mathbf{x}\in\Omega}|\nabla\phi^{(1)}|^2 \quad \text{and} \quad A^{(2)} = 3\max_{\mathbf{x}\in\Omega}|\nabla\phi^{(2)}|^2,$$

respectively, both of which are computed from already available stage values. With this notation, the first-stage term takes the form

$$\frac{\delta \mathcal{E}_c(\phi^{(1)})}{\delta \phi} - \frac{\delta \mathcal{E}_e(\phi^n)}{\delta \phi} = \delta\Delta^2\phi^{(1)} - A^n\Delta\phi^{(1)} - \left(\nabla\cdot(|\nabla\phi^n|^2\nabla\phi^n) - (A^n+1)\Delta\phi^n\right).$$

The corresponding expressions for the second and third stages can be obtained in the same way.

Since A is chosen at each stage from already available quantities, it is independent of the unknown at the current stage. Hence, each stage remains linear. Moreover, since the required convexity conditions are satisfied by construction, the convex splitting structure is preserved at each stage of the SSP-IMEX-RK update, and the unconditional energy stability analysis can be carried out in the same manner.

The RK coefficients $a_{10}, a_{11}, a_{20}, a_{21}, a_{22}, b_1, b_2$ are chosen to satisfy the second-order conditions:

$$\begin{cases}
a_{10} + a_{11} = 1,\\
a_{20} + a_{21} + a_{22} = 1,\\
a_{21} + a_{22}a_{11} + a_{22}b_1 + b_2 = 1,\\
a_{21} + a_{22}a_{11} + a_{22}a_{11}b_1 + a_{22}b_1^2 + a_{21}b_2 + a_{22}a_{11}b_2 + a_{22}b_1b_2 + b_2^2 = \frac{1}{2},\\
a_{22}b_1 + a_{11}b_2 + b_1b_2 = \frac{1}{2}.
\end{cases}$$

Letting $b_1 = b_2 = b\ (>0)$ yields $a_{10} = a_{20} = b - \frac{1}{2b}$, $a_{11} = -b + \frac{1}{2b} + 1$, $a_{21} = -b + \frac{1}{2b} + 2$, and $a_{22} = -1$, i.e.,

$$\begin{aligned}
\phi^{(1)} &= \phi^n - \Delta t\left(\frac{\delta \mathcal{E}_c(\phi^{(1)})}{\delta \phi} - \frac{\delta \mathcal{E}_e(\phi^n)}{\delta \phi}\right),\\
\phi^{(2)} &= \left(b - \frac{1}{2b}\right)\phi^n + \left(-b + \frac{1}{2b} + 1\right)\phi^{(1)} - b\Delta t\left(\frac{\delta \mathcal{E}_c(\phi^{(2)})}{\delta \phi} - \frac{\delta \mathcal{E}_e(\phi^{(1)})}{\delta \phi}\right),\\
\phi^{n+1} &= \left(b - \frac{1}{2b}\right)\phi^n + \left(-b + \frac{1}{2b} + 2\right)\phi^{(1)} - \phi^{(2)} - b\Delta t\left(\frac{\delta \mathcal{E}_c(\phi^{n+1})}{\delta \phi} - \frac{\delta \mathcal{E}_e(\phi^{(2)})}{\delta \phi}\right).
\end{aligned} \tag{2.2}$$

Lemma 2. *Let*

$$\underline{b} = 1 + \frac{\sqrt{r_1 + r_2 + 14}}{8\sqrt{3}} - \frac{1}{2}\sqrt{\frac{20\sqrt{3}}{\sqrt{r_1 + r_2 + 14}} - \frac{1}{12}r_1 - \frac{1}{3}r_2 + \frac{28}{3}}$$

and

$$\overline{b} = 1 + \frac{\sqrt{r_1 + r_2 + 14}}{8\sqrt{3}} + \frac{1}{2}\sqrt{\frac{20\sqrt{3}}{\sqrt{r_1 + r_2 + 14}} - \frac{1}{12}r_1 - \frac{1}{3}r_2 + \frac{28}{3}},$$

where $r_1 = \sqrt[3]{2(31 - 3\sqrt{105})}$ *and* $r_2 = \sqrt[3]{2(31 + 3\sqrt{105})}$. *For* $\underline{b} \le b \le \overline{b}$, *the following matrix induces a positive semi-definite quadratic form:*

$$\mathbf{M} = \begin{pmatrix} 1 & 0 & 0 \\ 2 & 1 & 0 \\ b - \frac{1}{2b} & b - \frac{1}{2b} & b \end{pmatrix}.$$

Proof. Since the skew-symmetric part of $\mathbf{M}$ does not contribute to the quadratic form, it suffices to consider the symmetric part $\frac{\mathbf{M}+\mathbf{M}^T}{2}$. Indeed, for any vector $\mathbf{z}$, $\mathbf{z}^T\mathbf{M}\mathbf{z} = \mathbf{z}^T\frac{\mathbf{M}+\mathbf{M}^T}{2}\mathbf{z}$. The eigenvalues of $\frac{\mathbf{M}+\mathbf{M}^T}{2}$ are $\lambda_1 = 0$, $\lambda_2 = \frac{b}{2} + 1 - \frac{\sqrt{12b^4 - 16b^3 + 8b^2 + 2}}{4b}$, and $\lambda_3 = \frac{b}{2} + 1 + \frac{\sqrt{12b^4 - 16b^3 + 8b^2 + 2}}{4b}$. Since $\lambda_1 = 0$ and $\lambda_3 \ge 0$, $\frac{\mathbf{M}+\mathbf{M}^T}{2}$ is positive semi-definite if and only if $\lambda_2 \ge 0$. Solving the inequality $\lambda_2 \ge 0$ yields $\underline{b} \le b \le \overline{b}$. Therefore, for $\underline{b} \le b \le \overline{b}$, $\mathbf{M}$ induces a positive semi-definite quadratic form. □

Remark 1. *Under the choice* $b_1 = b_2 = b$, *the second-order conditions determine the remaining RK coefficients in terms of the single free parameter b, and this leads to the scheme* (2.2). *The bounds* $\underline{b}$ *and* $\overline{b}$ *are then derived by requiring the quadratic form appearing in the discrete energy estimate to be nonnegative (see the proof of Theorem 1). Equivalently, b must be chosen so that* $\mathbf{M}$ *induces a positive semi-definite quadratic form. This yields the admissible range* $\underline{b} \le b \le \overline{b}$.

Before proving the decay property of the original discrete energy, we note that the intermediate energy terms $\mathcal{E}(\phi^{(1)})$ and $\mathcal{E}(\phi^{(2)})$ arise naturally from the multistage structure of the SSP-IMEX-RK method. Since the convex splitting structure is preserved at each stage, the convexity inequality can be successively applied to the stage values, and the resulting stage-wise estimates lead to the final discrete energy decay.

Theorem 1. *For* $\underline{b} \le b \le \overline{b}$, *the scheme* (2.2) *satisfies the original discrete energy decay property:*

$$\mathcal{E}(\phi^{n+1}) \le \mathcal{E}(\phi^n).$$

Proof. The convexity of $\mathcal{E}_c(\phi)$ and $\mathcal{E}_e(\phi)$ gives the following inequality:

$$\mathcal{E}(\phi) - \mathcal{E}(\psi) \le \int_\Omega \left(\frac{\delta\mathcal{E}_c(\phi)}{\delta\phi} - \frac{\delta\mathcal{E}_e(\psi)}{\delta\phi}\right)(\phi - \psi)\, d\mathbf{x}.$$

Using the inequality, we have

$$\mathcal{E}(\phi^{n+1}) - \mathcal{E}(\phi^n)$$

$$
\begin{aligned}
&= \left(\mathcal{E}(\phi^{n+1}) - \mathcal{E}(\phi^{(2)})\right) + \left(\mathcal{E}(\phi^{(2)}) - \mathcal{E}(\phi^{(1)})\right) + \left(\mathcal{E}(\phi^{(1)}) - \mathcal{E}(\phi^{n})\right) \\
&\leq \int_\Omega \left(\left(\frac{\delta \mathcal{E}_c(\phi^{n+1})}{\delta \phi} - \frac{\delta \mathcal{E}_e(\phi^{(2)})}{\delta \phi} \right)(\phi^{n+1} - \phi^{(2)}) + \left(\frac{\delta \mathcal{E}_c(\phi^{(2)})}{\delta \phi} - \frac{\delta \mathcal{E}_e(\phi^{(1)})}{\delta \phi} \right)(\phi^{(2)} - \phi^{(1)}) \right. \\
&\qquad \left. + \left(\frac{\delta \mathcal{E}_c(\phi^{(1)})}{\delta \phi} - \frac{\delta \mathcal{E}_e(\phi^{n})}{\delta \phi} \right)(\phi^{(1)} - \phi^{n}) \right) d\mathbf{x} \\
&= -\frac{1}{b\Delta t} \int_\Omega \left(\left(\phi^{n+1} - \phi^{(2)} + 2(\phi^{(2)} - \phi^{(1)}) + \left(b - \frac{1}{2b} \right)(\phi^{(1)} - \phi^{n}) \right)(\phi^{n+1} - \phi^{(2)}) \right. \\
&\qquad \left. + \left(\phi^{(2)} - \phi^{(1)} + \left(b - \frac{1}{2b} \right)(\phi^{(1)} - \phi^{n}) \right)(\phi^{(2)} - \phi^{(1)}) + b(\phi^{(1)} - \phi^{n})^2 \right) d\mathbf{x} \\
&= -\frac{1}{b\Delta t} \int_\Omega (\phi^{n+1} - \phi^{(2)}, \phi^{(2)} - \phi^{(1)}, \phi^{(1)} - \phi^{n}) \mathbf{M} (\phi^{n+1} - \phi^{(2)}, \phi^{(2)} - \phi^{(1)}, \phi^{(1)} - \phi^{n})^T \, d\mathbf{x} \\
&\leq 0.
\end{aligned}
$$

□

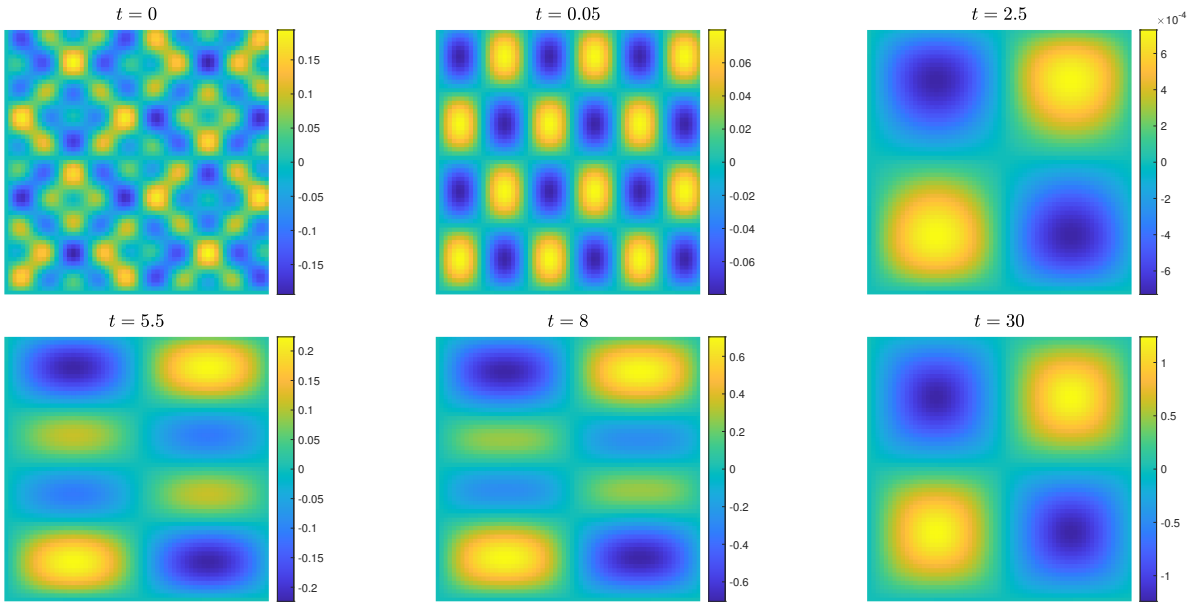

(a)

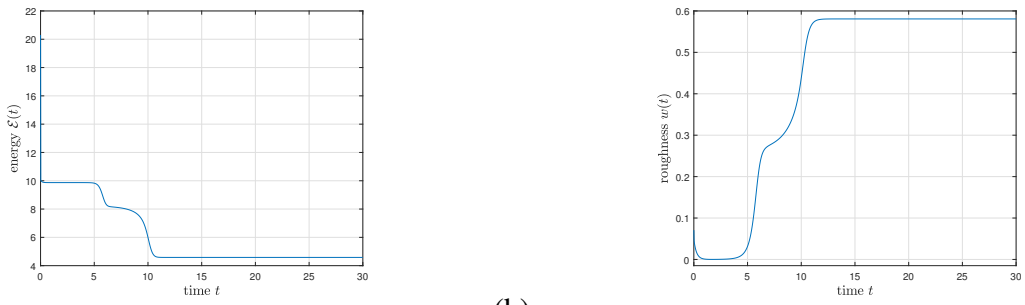

(b)

Figure 1. Evolution of (a) $\phi(x, y, t)$ and (b) its $\mathcal{E}(t)$ (left) and $w(t)$ (right) with $\delta = 0.1$.

3. Numerical results

The spatial domain is discretized using the Fourier spectral method. Since the slope-selection epitaxial thin-film growth equation is not an interfacial model such as the Cahn–Hilliard equation, the usual transition-layer resolution criterion is not directly applicable here. Instead, the adequacy of the spatial resolution is verified through additional spatial refinement tests, which show that, for sufficiently fine Fourier discretizations, further spatial refinement has a negligible effect on the measured errors; see Appendix and Figure 8.

3.1. Accuracy, computational efficiency, and energy stability

We verify the accuracy, computational efficiency, and energy stability of the proposed scheme using the following initial condition [3]:

$$\phi(x, y, 0) = 0.1\,(\sin 3x \sin 2y + \sin 5x \sin 5y)$$

with $\Omega = [0, 2\pi]^2$, $\delta = 0.1$, and $\Delta x = \Delta y = \frac{2\pi}{64}$. Figures 1 (a) and (b) show the evolution of $\phi(x, y, t)$ and its $\mathcal{E}(t)$ and $w(t)$, respectively, with $b = 0.4$ and $\Delta t = 0.01 \cdot 2^{-9}$. Figures 2 (a) and (b) show the relative l_2-errors of $\phi(x, y, t)$ at $t = 2.5$ and 5.5 and the central processing unit (CPU) times for the scheme, respectively, with $b = 0.4$, 1.3, 2.3, 3.3, and 4.2 for $\Delta t = 0.01 \cdot 2^{-7}, 0.01 \cdot 2^{-6}, \ldots, 0.01$. The errors are computed with respect to the reference solution obtained using $\Delta t = 0.01 \cdot 2^{-9}$, and the CPU times are measured on an Intel Core i5-14400 CPU at 2.50GHz with 8GB RAM. It is observed that the scheme achieves second-order convergence in time, and the CPU time scales almost linearly with the number of time steps, independently of b.

We also perform simulations using larger time steps. Figure 3 shows the evolution of $\mathcal{E}(t)$ with $b = 0.4$, 1.3, 2.3, 3.3, and 4.2 for $\Delta t = 0.000625$, 0.0025, 0.01, 0.1, 1, and 10. As proved in Theorem 1, the energy does not increase in time for $\underline{b} \le b \le \overline{b}$. Based on the results in Figures 2 and 3, we fix $b = 0.4$ and $\Delta t = 0.0025$ for the remainder of the paper.

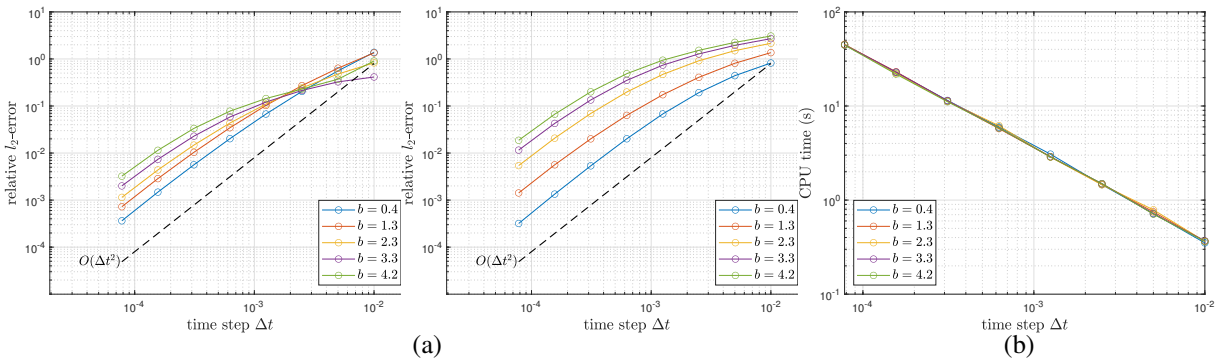

(a) (b)

Figure 2. (a) relative l_2-errors of $\phi(x, y, t)$ at $t = 2.5$ (left) and 5.5 (right) and (b) CPU times with different values of b for various Δt.

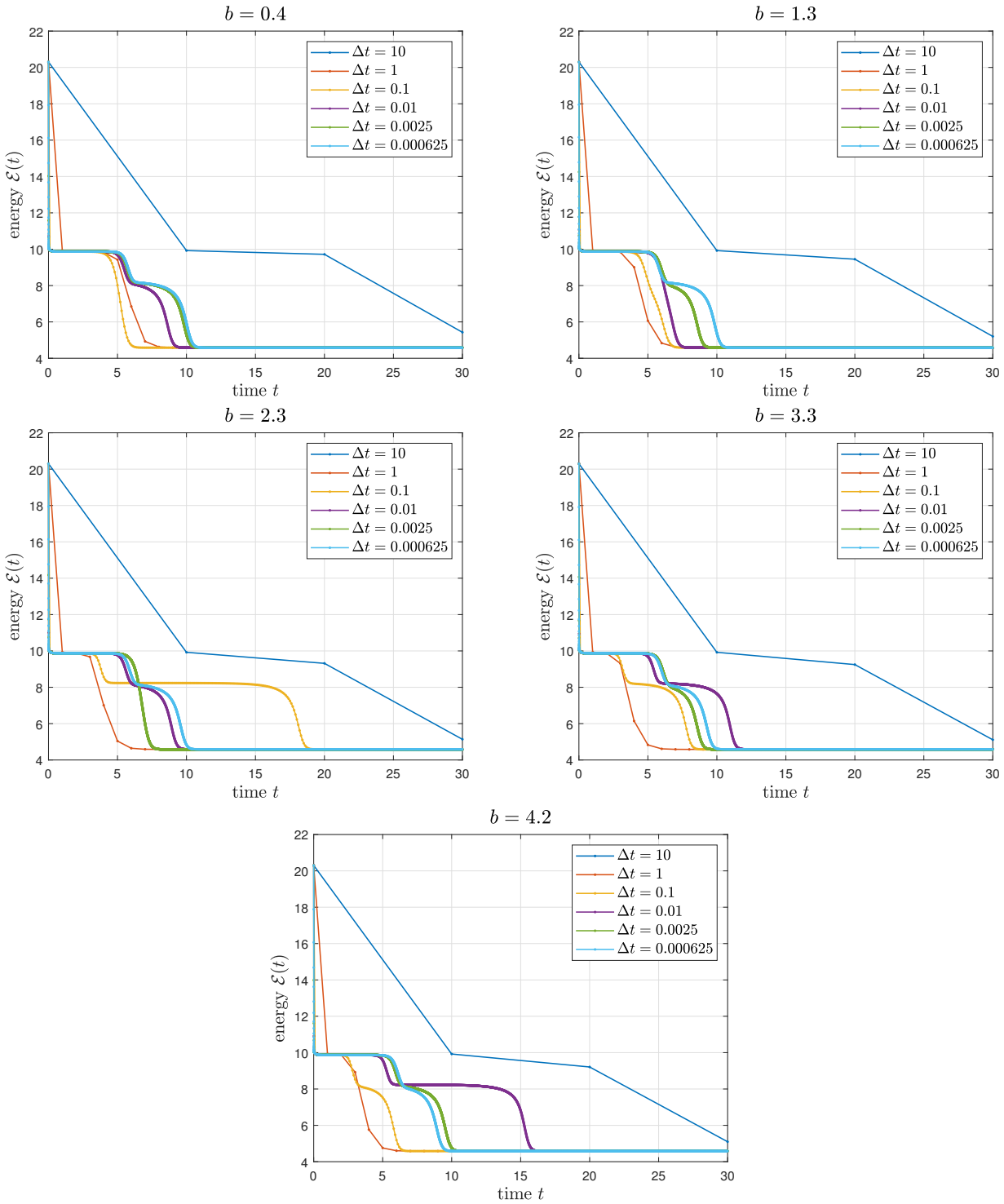

Figure 3. Evolution of $\mathcal{E}(t)$ with different values of b for various Δt.

3.2. Coarsening dynamics

To evaluate the applicability of the scheme to simulating coarsening dynamics, we take an initial condition as follows:

$$\phi(x, y, 0) = \text{rand}(x, y),$$

where $\text{rand}(x, y)$ is a uniformly distributed random number in the interval $[-0.001, 0.001]$. We use $\Omega = [0, 12.8]^2$ and $\Delta x = \Delta y = \frac{12.8}{512}$ to resolve small-scale structures in the numerical solution. Figures 4–6 show the evolution of $\phi(x, y, t)$ and its Laplacian with $\delta = 0.03^2$, 0.06^2, and 0.1^2, respectively. The coarsening dynamics and the evolution of hill-and-valley structures become apparent, and the coarsening speed exhibits a clear dependence on δ. Figure 7 shows the evolution of $\mathcal{E}(t)$ and $w(t)$, where the energy decays like $t^{-\frac{1}{3}}$ and the roughness grows like $t^{\frac{1}{3}}$. The results in Figures 4–7 indicate that the proposed scheme demonstrates long-time accuracy and energy stability, and is therefore suitable for simulating coarsening dynamics.

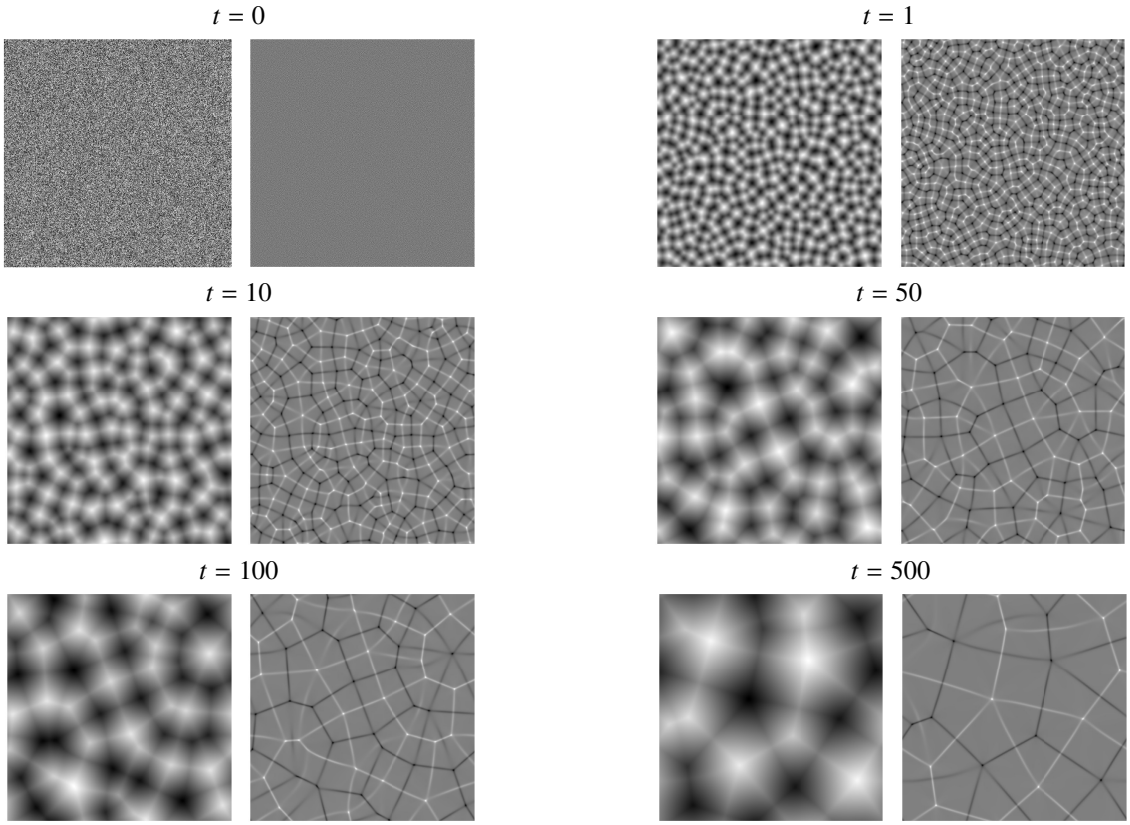

Figure 4. Evolution of $\phi(x, y, t)$ (left) and its Laplacian (right) with $\delta = 0.03^2$.

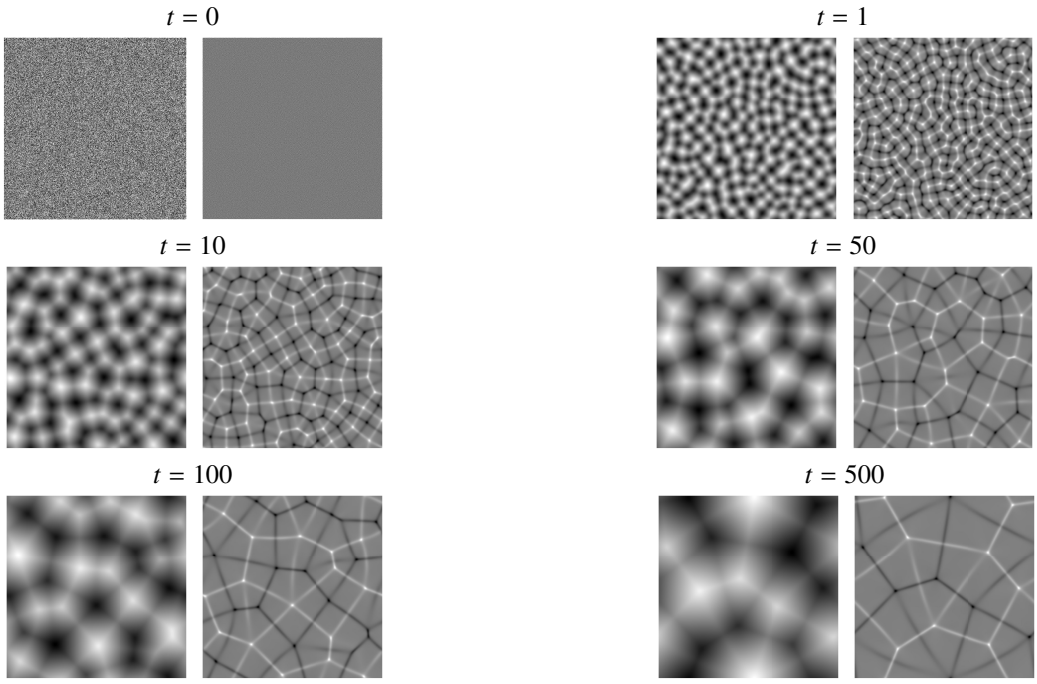

Figure 5. Evolution of $\phi(x, y, t)$ (left) and its Laplacian (right) with $\delta = 0.06^2$.

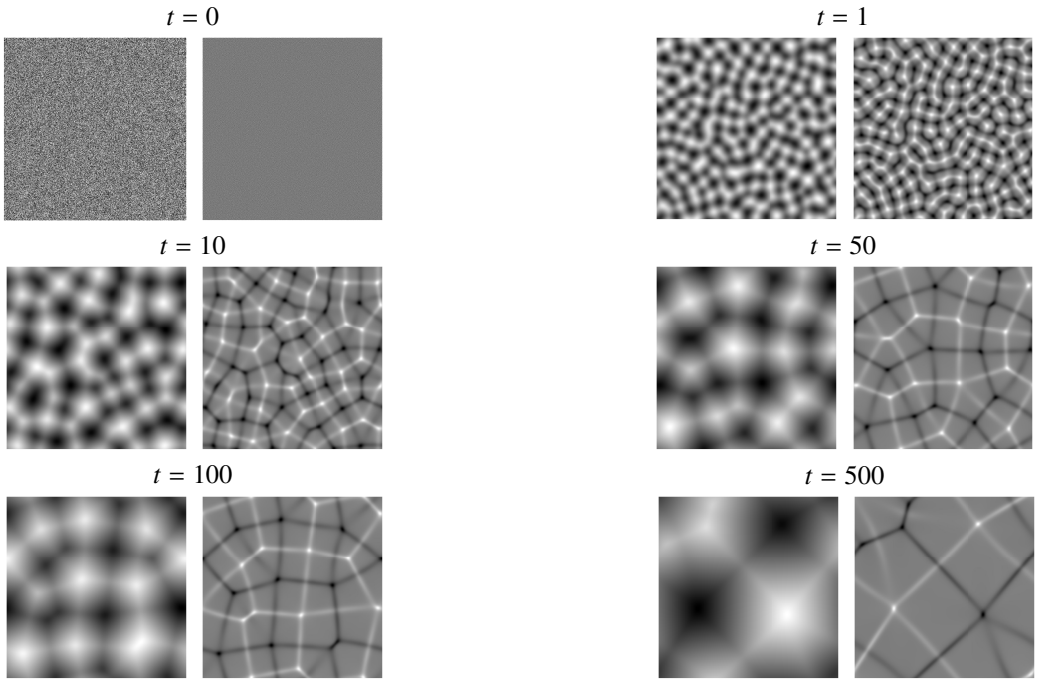

Figure 6. Evolution of $\phi(x, y, t)$ (left) and its Laplacian (right) with $\delta = 0.1^2$.

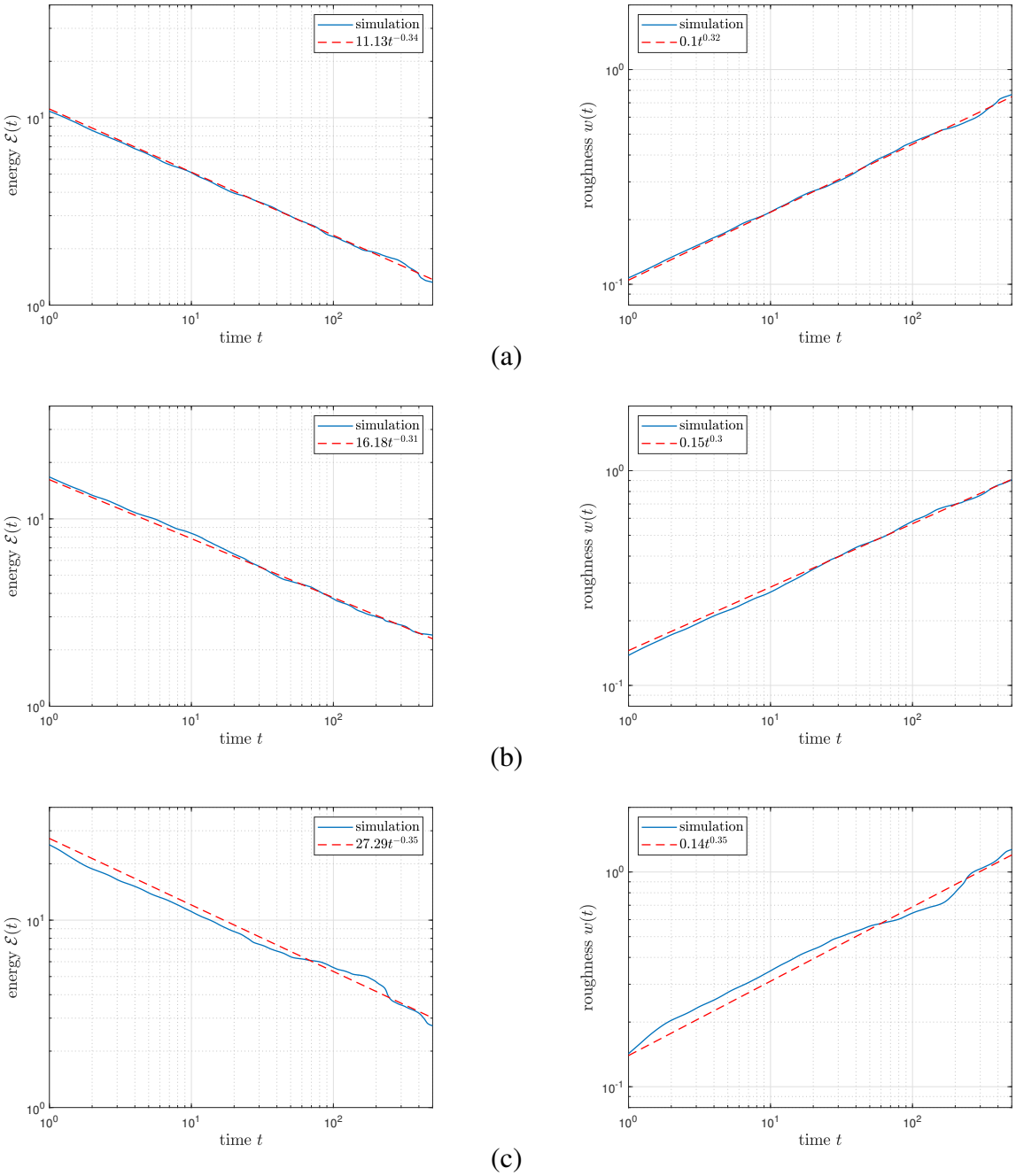

Figure 7. Evolution of $\mathcal{E}(t)$ (left) and $w(t)$ (right) with (a) $\delta = 0.03^2$, (b) 0.06^2, and (c) 0.1^2. In each figure, the solid line represents the simulation result, whereas the dashed line corresponds to its least-squares fit.

4. Conclusions

We developed a second-order, linear, and energy-stable scheme for the SS equation. The scheme was constructed by combining a linear convex splitting of the original energy functional with a second-order SSP-IMEX-RK method. For $\underline{b} \le b \le \overline{b}$, we proved that the scheme is unconditionally energy-stable with respect to the original discrete energy functional.

Numerical experiments confirmed that the scheme achieves second-order convergence in time, is computationally efficient, and preserves the original discrete energy decay property. Furthermore, long-time simulations of coarsening dynamics demonstrated that the scheme accurately captures the expected scaling laws, indicating its effectiveness and robustness for the SS model.

We also note that b is the single free parameter within the admissible range $\underline{b} \le b \le \overline{b}$. For any choice of b in this range, the original discrete energy decay property is guaranteed theoretically. The numerical results also show that the CPU times are nearly identical for different admissible values of b. Although the observed convergence order remains second order for the tested admissible values of b, the choice of b may affect the error constant. A rigorous characterization of how the error constant depends on b, and hence the identification of an optimal choice of b, remains an interesting topic for future work.

Appendix

MATLAB code

The MATLAB code for the scheme (2.2) used to generate Figure 4 is given below.

```
x1=0; xr=12.8; y1=0; yr=12.8; T=500; Δ=0.03^2; b=0.4; nx=512; ny=512; dt=0.0025;

dx=(xr-x1)/nx; dy=(yr-y1)/ny; x=x1:dx:xr-dx; y=y1:dy:yr-dy;
xix=1i*2*pi*fftshift(-nx/2:nx/2-1)/(xr-x1); xiy=1i*2*pi*fftshift(-ny/2:ny/2-1)/(yr-y1);
[xiX,xiY]=ndgrid(xix,xiy); xi_lap=xiX.^2+xiY.^2; nt=round(T/dt);

ophi=0.001*(2*rand(nx,ny)-1);
for it=1:nt
    Phin = fft2(ophi);
    [An,Ftn] = comp_A(Phin,xiX,xiY); Rhsn = Phin + dt*(Ftn-(An+1)*xi_lap.*Phin);
    Phi1 = Rhsn./(1+dt*(Δ*xi_lap.^2-An*xi_lap));

    [A1,Ft1] = comp_A(Phi1,xiX,xiY);
    Rhs1 = (b-1/(2*b))*Phin + (-b+1/(2*b)+1)*Phi1 + b*dt*(Ft1-(A1+1)*xi_lap.*Phi1);
    Phi2 = Rhs1./(1+b*dt*(Δ*xi_lap.^2-A1*xi_lap));

    [A2,Ft2] = comp_A(Phi2,xiX,xiY);
    Rhs2 = (b-1/(2*b))*Phin + (-b+1/(2*b)+2)*Phi1 - Phi2 + b*dt*(Ft2-(A2+1)*xi_lap.*Phi2);
    nphi = real(ifft2(Rhs2./(1+b*dt*(Δ*xi_lap.^2-A2*xi_lap))));
    ophi = nphi;
end

function [A,Ft] = comp_A(Phi,xiX,xiY)
phix = real(ifft2(xiX.*Phi)); phiy = real(ifft2(xiY.*Phi)); gradphi_sq = phix.^2+phiy.^2;
A = 3*max(gradphi_sq(:));
Ft = xiX.*fft2(gradphi_sq.*phix)+xiY.*fft2(gradphi_sq.*phiy);
end
```

Spatial refinement study

To verify the adequacy of the spatial resolution, we perform additional spatial refinement tests using the parameter set from Section 3.1, while varying only the number of grid points N. Figure 8 shows the relative l_2-errors of $\phi(x, y, 2.5)$ for $N = 16$, 24, 32, 48, 64, 96, and 128, with the same values of b and Δt as in Section 3.1. The errors are computed with respect to the reference solution obtained using $N = 256$ and $\Delta t = 0.01 \cdot 2^{-9}$. In each subfigure, the vertical dashed line indicates the spatial resolution used in the main computations. For sufficiently fine Fourier discretizations, further spatial refinement has a negligible effect on the measured errors.

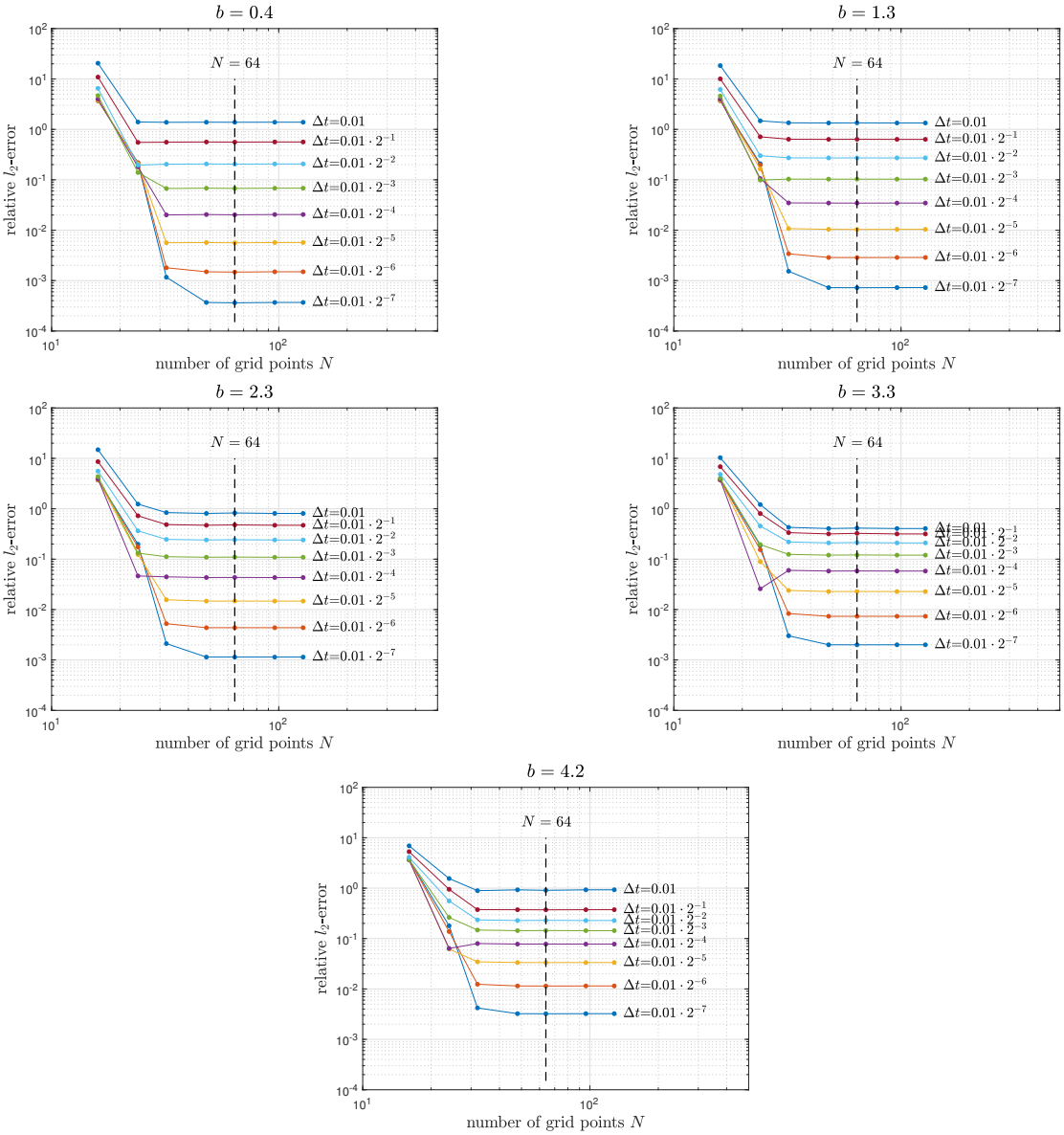

Figure 8. Relative l_2-errors of $\phi(x, y, 2.5)$ with different values of b for various N and Δt.

Use of Generative-AI tools declaration

The author declares they have not used Artificial Intelligence (AI) tools in the creation of this article.

Acknowledgments

The corresponding author (H.G. Lee) was supported by the National Research Foundation of Korea (NRF) grant funded by the Korea government (MSIT) (No. RS-2022-NR069708, RS-2025-00562688).

Conflict of interest

The author declares that there is no conflicts of interest.

References

1. M. Ortiz, E.A. Repetto, H. Si, A continuum model of kinetic roughening and coarsening in thin films, *J. Mech. Phys. Solids*, **47** (1999), 697–730. https://doi.org/10.1016/S0022-5096(98)00102-1
2. D. Moldovan, L. Golubović, Interfacial coarsening dynamics in epitaxial growth with slope selection, *Phys. Rev. E*, **61** (2000), 6190–6214. https://doi.org/10.1103/PhysRevE.61.6190
3. B. Li, J.-G. Liu, Thin film epitaxy with or without slope selection, *Eur. J. Appl. Math.*, **14** (2003), 713–743. https://doi.org/10.1017/S0956792503003764
4. J. Shen, C. Wang, X. Wang, S. M. Wise, Second-order convex splitting schemes for gradient flows with Ehrlich–Schwoebel type energy: Application to thin film epitaxy, *SIAM J. Numer. Anal.*, **50** (2012), 105–125. https://doi.org/10.1137/110837841
5. D.J. Eyre, Unconditionally gradient stable time marching the Cahn–Hilliard equation, *MRS Proc.*, **529** (1998), 39–46. https://doi.org/10.1557/PROC-529-39
6. Q. Du, R. A. Nicolaides, Numerical analysis of a continuum model of phase transition, *SIAM J. Numer. Anal.*, **28** (1991), 1310–1322. https://doi.org/10.1137/0728091
7. X. Yang, J. Zhao, Q. Wang, Numerical approximations for the molecular beam epitaxial growth model based on the invariant energy quadratization method, *J. Comput. Phys.*, **333** (2017), 104–127. https://doi.org/10.1016/j.jcp.2016.12.040
8. X. Yang, Linear, first and second-order, unconditionally energy stable numerical schemes for the phase field model of homopolymer blends, *J. Comput. Phys.*, **327** (2016), 294–316. https://doi.org/10.1016/j.jcp.2016.08.011
9. W. Feng, C. Wang, S. M. Wise, Z. Zhang, A second-order energy stable backward differentiation formula method for the epitaxial thin film equation with slope selection, *Numer. Methods Partial Differential Eq.*, **34** (2018), 1975–2007. https://doi.org/10.1002/num.22378
10. Q. Cheng, J. Shen, X. Yang, Highly efficient and accurate numerical schemes for the epitaxial thin film growth models by using the SAV approach, *J. Sci. Comput.*, **78** (2019), 1467–1487. https://doi.org/10.1007/s10915-018-0853-6

11. J. Shen, J. Xu, J. Yang, The scalar auxiliary variable (SAV) approach for gradient flows, *J. Comput. Phys.*, **353** (2018), 407–416. https://doi.org/10.1016/j.jcp.2017.10.066

12. K. Glasner, S. Orizaga, Improving the accuracy of convexity splitting methods for gradient flow equations, *J. Comput. Phys.*, **315** (2016), 52–64. https://doi.org/10.1016/j.jcp.2016.03.042

13. S. Orizaga, T. Witelski, IMEX methods for thin-film equations and Cahn–Hilliard equations with variable mobility, *Comput. Mater. Sci.* **243** (2024), 113145. https://doi.org/10.1016/j.commatsci.2024.113145

14. H. Song, Energy SSP-IMEX Runge–Kutta methods for the Cahn–Hilliard equation, *J. Comput. Appl. Math.*, **292** (2016), 576–590. https://doi.org/10.1016/j.cam.2015.07.039

15. H.G. Lee, Stability condition of the second-order SSP-IMEX-RK method for the Cahn–Hilliard equation, *Mathematics*, **8** (2020), 11. https://doi.org/10.3390/math8010011

AIMS Press